Quantum phase transition as an interplay of Kitaev and Ising interactions

A. Langari,[1,2,3,*] A. Mohammad-Aghaei,[1] and R. Haghshenas[1]

[1]*Department of Physics, Sharif University of Technology, P.O. Box 11155-9161, Tehran, Iran*

[2]*Center of excellence in Complex Systems and Condensed Matter (CSCM), Sharif University of Technology, Tehran 1458889694, Iran*

[3]*Max-Planck-Institut für Physik komplexer Systeme, D-01187 Dresden, Germany*

(Received 10 August 2014; revised manuscript received 18 December 2014; published 15 January 2015)

We study the interplay between the Kitaev and Ising interactions on a ladder geometry. We show that the ground state of the Kitaev ladder is a symmetry-protected topological (SPT) phase, which is protected by a $\mathbb{Z}_2 \times \mathbb{Z}_2$ symmetry. The nature of the SPT phase is confirmed by degeneracy of the entanglement spectrum. Nonlocal order parameters that indirectly measure phase factors (inequivalent projective representations of the symmetries) of the $\mathbb{Z}_2 \times \mathbb{Z}_2$ symmetry explicitly show the protection of the SPT phase under the $\mathbb{Z}_2 \times \mathbb{Z}_2$ symmetry. We derive the effective theory to describe the topological phase transition on the ladder geometry, which is given by a transverse field Ising model with/without next-nearest-neighbor coupling based on the primary Ising configurations. The ladder has three phases, namely, the Kitaev SPT, symmetry-broken ferro/antiferromagnetic order, and classical spin liquid. The nonzero quantum critical point and its corresponding central charge are provided by the effective theory, which are in full agreement with the numerical results, i.e., the divergence of entanglement entropy at the critical point and change of the entanglement spectrum degeneracy. The central charge of the critical points are either $c = 1$ or $c = 2$, with the magnetization and correlation exponents being $1/4$ and $1/2$, respectively. The transition from the classical spin-liquid phase of the frustrated Ising ladder to the Kitaev SPT phase is mediated by a floating phase, which shows strong finite entanglement scaling.

DOI: 10.1103/PhysRevB.91.024415 PACS number(s): 05.30.Rt, 75.10.Jm, 03.67.−a

I. INTRODUCTION

Topologically ordered quantum many-body systems have received a great deal of interest due to rich insights emerged from their nature, namely, lack of any local order parameter to characterize them [1,2], i.e., failure of symmetry-breaking paradigm, exhibiting long-range entanglement [3], robustness against local perturbations [4,5], nontrivial anyon statistics [6,7], and so on. Topological quantum codes including color codes [8–11] have a universal feature characterized by topological entanglement entropy [12,13] manifesting their topological nature. Emergent fermions and anyons [14–16] are typical quasiparticle excitations above a topological ground state that influence the finite temperature properties with nontrivial limiting features [17] and bound states [18]. The stability of the topological ordered state against the thermal, external magnetic field [19] and other interactions [20] (like Ising [21]) is an interesting issue, which could lead to the phase transition from a topological state. For instance, an in-plane magnetic field on the toric code leads to both first- and second-order quantum phase transition [22], while a perpendicular magnetic field gives a first-order phase transition at the self-dual point of the effective quantum compass model [23]. The two-dimensional (2D) color code shows similar behavior in the presence of a magnetic field [24] and Ising interactions [25]. The nature of such a phase transition and its corresponding quantum critical properties are debating issues inherited from the topological properties of the model.

Recently, many efforts, inspired by the concepts of quantum information theory, have been made to provide a comprehensive understanding of topological order [26–28]. So far, it is believed that there exist three different kinds of topological orders, namely: symmetry-protected topological (SPT) order, long-range entangled states with topological order, and symmetry-enriched topological order. The SPT orders or SPT phases are of a short-range entanglement type and totally characterized by some symmetries. Theses symmetries protect the SPT phase: The SPT phase is stable as far as the symmetries are being preserved. The mechanism that determines which symmetries protect the phase is called symmetry fractionalization. In other words, symmetry fractionalization provides a recipe, based on matrix-product state (MPS) representation of the ground state, to determine a set of unique labels for the SPT phase—for more explanation, see Ref. [29]. Symmetry fractionalization theory in one dimension is complete and thoroughly characterizes the SPT phases. In higher dimensions, it is believed that symmetry fractionalization, symmetry breaking, and long-range entanglement mechanisms are capable of characterizing the aforementioned orders. However, to get a complete understanding, further studies are currently active and demanding.

Characterization of topological order relies on appropriate nonlocal order parameters. In one dimension, the entanglement spectrum distinguishes SPT orders from trivial ones [26], while nonlocal order parameters based on inequivalent projective representations [30] identify different SPT orders [31]. In two dimensions, even so, there is not a unique and faithful tool to classify them but topological entanglement entropy [13] is assumed as the most common tool to characterize intrinsic topological phases. The case of symmetry-enriched topological orders is more complicated as both orders, i.e., SPT and intrinsic topological orders, simultaneously exist—some proposed nonlocal measures might hopefully identify them [32,33]. Understanding a quantum phase transition (QPT) from a topological phase to a trivial phase requires less effort than the classification of phases, since local-order parameters according to the symmetry-breaking mechanism can identify the quantum phase transition. Novel quantum

*langari@sharif.edu

phase transitions, which rarely have been studied, happen when there are two distinct topological phases.

In this article, we consider the Kitaev toric code model accompanied by different Ising interactions, namely, rhombic-Ising (RI), leg-Ising (LI), and rhombic-leg-Ising (RLI) interactions, on ladder geometry. The nonfrustrated RI case of ladder geometry has been studied recently in Ref. [21]. Here, we consider all possible Ising interactions, which include the frustrated model on the ladder structure. The Kitaev-toric code [5] is a well-known model showing topological order, while the Ising model with respect to the geometry of lattice and the type of interactions can show symmetry-broken phases and spin-liquid phases [34]. The latter is due to the frustration of antiferromagnetic (AF) interactions of the Ising model (AF RLI interactions), which leads to a rich phase diagram [35–43]. It should be mentioned that the Kitaev-toric code discussed here is different from the Kitaev-honeycomb model [44] which has been studied on both ladder and 2D structures [45–47].

We show that the ground state of the Kitaev ladder is an SPT phase by introducing the responsible $\mathbb{Z}_2 \times \mathbb{Z}_2$ symmetries, which is confirmed by numerical results on the corresponding nontrivial phase factor [31]—see Appendix B. To investigate the competition between the Kitaev SPT phase and an Ising phase we employ two general approaches: an effective theory, which comes from an exact map of the original model to an effective one, and the infinite system density-matrix-renormalization-group (iDMRG) algorithm [48–50] based on infinite matrix product state (iMPS) representation. On the ladder geometry, the Kitaev plus Ising interactions are mapped to decoupled chains of the nearest-neighbor (NN) with/without next-nearest-neighbor (NNN) transverse field Ising (TFI) model. The effective theory and numerical iDMRG computations show a quantum phase transition at finite nonzero coupling from the Kitaev SPT phase to the broken symmetry antiferro/ferromagnetic phase except in the case of AF RLI interactions. The existence of quantum critical point (QCP) and its location is proved by numerical simulation that leads to the divergence of the entanglement entropy, change in the degeneracy of the entanglement spectrum, change of phase factor, and the nonzero magnetic order parameter. We have also computed the corresponding central charges, which is in agreement with the proposed effective theory, namely, $c = 2$ for Kitaev-LI, $c = 1$ for both Kitaev-RI and Kitaev-RLI QCPs. The critical exponents of magnetization and correlation function are $\beta = 1/4$ and $\eta = 1/2$, correspondingly for all types of nonfrustrated ladders. Concerning the QCP, our result for Kitaev-RI interactions is in contrast to Ref. [21], which concludes zero Ising coupling strength, while we observe a finite nonzero Ising coupling ($J_z = J_v$; see Fig. 6). Moreover, the whole study for the LI and RLI cases are new investigations of this manuscript that include the frustrated case. The case of AF RLI coupling makes a competition between the Kitaev SPT phase and a classical spin-liquid one, which can be explained in terms of the frustrated NNN TFI effective theory. Our numerical results for the AF RLI case are in favor of the existence of a floating phase—which has algebraic decaying correlations—between the classical spin-liquid and Kitaev SPT phases. This is in agreement with the phase diagram proposed for the (effective) frustrated NNN TFI chain in Refs. [41,42].

The remainder of this paper is organized as follows. In Sec. II we first briefly review the Kitaev toric code on ladder and introduce the $\mathbb{Z}_2 \times \mathbb{Z}_2$ symmetry, which protects the degeneracy of the entanglement spectrum. We then define different types of Ising interactions in Sec. III and derive the effective theory for the Kitaev-Ising interplay. We present our numerical results in the same section. Finally in Sec. IV, we end up with a summary and discussion. The article is accompanied by two appendixes, which describe the underlying numerical iDMRG (iMPS) approach.

II. THE SPT PHASE OF KITAEV LADDER

The Kitaev ladder is defined on the ladder geometry as shown in Fig. 1, where the spins sit on the bonds of the two-leg ladder. The Kitaev Hamiltonian ($\mathcal{H}_\mathcal{K}$) is composed of two terms, vertex (A_v) and plaquette (B_p) interactions,

$$\begin{aligned} \mathcal{H}_\mathcal{K} &= -J_v \sum_{\perp,\top} A_v - J_p \sum_{\square} B_p, \\ A_v &\equiv \prod_i \sigma_i^x, i \in \perp \text{ or } \top ; J_v > 0, \\ B_p &\equiv \prod_j \sigma_j^z, j \in \square ; J_p > 0, \end{aligned} \tag{1}$$

where σ_j^α is the α-component Pauli matrix at position j. The model is exactly solvable [51], which has twofold topologically degenerate ground states. Let $|\Omega\rangle \equiv \otimes_i |+\rangle_i$, where $|+\rangle_i$ is the eigenstate of σ_i^x; a ground state of the Kitaev ladder is given by

$$|\psi_K\rangle = \frac{1}{2^N} \prod_p (1 + B_p)|\Omega\rangle, \tag{2}$$

where N is the total number of rungs on the ladder. And $|\psi'_K\rangle = W_z|\psi_K\rangle$ is the other ground state in which $W_z = \prod_\ell \sigma_\ell^z$, where ℓ runs only on one of the legs of the ladder. The ground state is understood as an equally weighted superposition of the states, which are obtained by the operation of any homologically trivial loop of σ^z operators on $|\Omega\rangle$. The excited states can be constructed by the operation of open strings of σ^z operators on $|\Omega\rangle$. A complete characterization of the spectrum shows that the excited states are at least twofold degenerate, which could be more except the highest energy level that has only a double degeneracy [51]. Moreover, the ground-state entropy of the model is equal to ln(2).

The Kitaev ladder ($\mathcal{H}_\mathcal{K}$) has (i) twofold degenerate ground state which cannot be distinguished by a local-order parameter

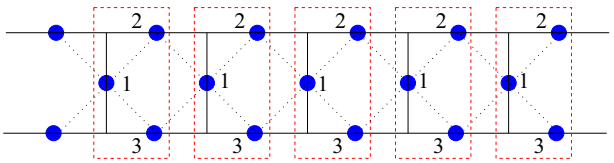

FIG. 1. (Color online) Two-leg Kitaev ladder, where the solid blue circles show the position of real spins. The triangles show the vertex term and rhombuses represent the plaquette term in the Hamiltonian. The dashed red rectangle shows the unit cell of the model.

of the Landau-Ginzburg symmetry-breaking paradigm, (ii) a finite-energy gap between the ground state and the first excited one, and (iii) anyonic excitations of integer magnetic and electric charges with Abelian statistics [51]. Although the quasi-one-dimensional Kitaev ladder does not bear topological characters like Wilson loops and topological entanglement entropy its ground state is classified to be an SPT phase. We will show explicitly that the ground state of the Kitaev ladder is protected by a $\mathbb{Z}_2 \times \mathbb{Z}_2$ symmetry. For each unit cell of the two-leg ladder, Fig. 1, the following operator is defined:

$$\Sigma^{abc}(j) = \sigma_1^a(j)\sigma_2^b(j)\sigma_3^c(j), \quad a,b,c = I,x,y,z, \tag{3}$$

where $\sigma_i^I(j)$ is the identity operator at position i of unit cell j. It is straightforward to show that $\mathcal{H}_\mathcal{K}$ is invariant under the operation of the following two operators:

$$\mathcal{X} = \prod_j \Sigma^{xxx}(j) \text{ and } \mathcal{Z} = \prod_j \Sigma^{Izz}(j), \tag{4}$$

where j runs over all unit cells. Moreover, $[\mathcal{X}, B_p] = 0$, which states that the ground state of the Kitaev ladder is invariant under $\mathcal{X}$. Similarly, it can be shown that the ground state of the Kitaev ladder is invariant under $\mathcal{Z}$, since the product of $\mathcal{Z}$ by $\prod_p(1+B_p)$ is equivalent to the operation of $\prod_p(1+B_p)$. Hence, the Kitaev-ladder ground state is invariant under the mutual symmetry operation $\mathcal{X} \times \mathcal{Z}$, which defines the mentioned $\mathbb{Z}_2 \times \mathbb{Z}_2$ symmetry. The local symmetry operation $\Sigma^{Izz}, \Sigma^{xxx}$, are two members of the group $G = \{\Sigma^{Izz}, \Sigma^{xxx}, -\Sigma^{xyy}, \Sigma^{III}\}$. According to Ref. [31], we exploit this property and define an order parameter $\mathcal{O}$, which can serve to detect which projective representation holds for the ground state in terms of its iMPS representation. The order parameter $\mathcal{O}$ is defined by

$$\mathcal{O} = \frac{1}{\chi}\mathrm{Tr}(U_g U_{g'} U_g^\dagger U_{g'}^\dagger), \quad g \in G, \tag{5}$$

where U_g comes from the transformation of the iMPS representation of the ground state (Γ_j) under the symmetry $\mathcal{X} \times \mathcal{Z}$, i.e., $\Gamma_j \to U_g^\dagger \Gamma_j U_g$, where $g \in G$ and χ is the dimension of matrices in iMPS (for details see Appendix B). The SPT, trivial, and symmetry-breaking phases are, respectively, characterized by $\mathcal{O} = \{-1,1,0\}$. Hereafter, $\mathcal{O}$ is called the "phase factor order parameter."

These kind of order parameters—as discussed in Refs. [31,52]—is generally realized by a string of unitary operations accompanied by some permutations. To show explicitly the form of Eq. (5) in terms of a nonlocal order parameter, we define $\varepsilon_m(\psi)$ as follows:

$$\mathcal{X}_m = (\Sigma^{xxx})^{\otimes m}, \mathcal{Z}_m = (\Sigma^{Izz})^{\otimes m}, \mathcal{I}_m = (\Sigma^{III})^{\otimes m},$$
$$\varepsilon_m(\psi) := \langle\psi|(\mathcal{Z}_m \otimes \mathcal{Z}_m \otimes \mathcal{I}_m)F_{13}(\mathcal{X}_m \otimes \mathcal{X}_m \otimes \mathcal{I}_m)|\psi\rangle,$$

where F_{13} swaps the first and third pack of sites, i.e.,

$$F_{13} : (\mathcal{X}_m \otimes \mathcal{X}_m \otimes \mathcal{I}_m) \longrightarrow (\mathcal{I}_m \otimes \mathcal{X}_m \otimes \mathcal{X}_m).$$

As shown in Ref. [52]— Cf. Fig. 2 and Eq. (2) of Ref. [52]— when m increases, $\varepsilon_m(\psi)$ exponentially converges to $\mathcal{O}$. Therefore, order parameter $\mathcal{O}$ could be calculated directly from an explicit expectation value, i.e., $\varepsilon_m(\psi)$, without using symmetric transformation of iMPS representation. We find numerically that the Kitaev phase reveals $\mathcal{O} = -1$, (see Fig. 10) which justifies that it is being protected by $\mathcal{X} \times \mathcal{Z}$ symmetries. Moreover, the entanglement spectrum is degenerate in the Kitaev phase (see Fig. 5), which confirms that the ground state of the Kitaev ladder is an SPT phase.

III. KITAEV-ISING LADDER

The Ising term, which is composed of two-body interactions, competes with the SPT character of the pure Kitaev ground state on the ladder. The Ising interaction $J_z\sigma_i^z\sigma_j^z$ (which is defined on the nearest-neighbor spins of ladder) does not commute with the vertex terms (A_v) of $\mathcal{H}_\mathcal{K}$, hence, it establishes a competition between a symmetry-protected topological phase and a classical state. The classical state, which is a result of strong Ising interaction could be realized in different forms according to the pattern of Ising interactions. We classify three types of Ising interactions on the two-leg ladder in Fig. 2: (a) Rhombic-Ising interactions, where the Ising terms are defined only between the nearest neighbor spins sitting on each rhombus [see Fig. 2(a)]. The corresponding Ising Hamiltonian ($\mathcal{H}_\mathcal{R}$) is defined in Eq. (8). (b) Leg-Ising interactions, which are defined between nearest-neighbor spins on the legs of the ladder as shown in Fig. 2(b) and given by $\mathcal{H}_\mathcal{L}$ in Eq. (22). (c) Rhombic-leg-Ising interactions that are composed of nearest-neighbor interaction between any pair of spins on the two-leg ladder, which is shown in Fig. 2(c) and is represented by the sum of two previous cases, i.e., $\mathcal{H}_{\mathcal{RL}} = \mathcal{H}_\mathcal{R} + \mathcal{H}_\mathcal{L}$. We consider both ferromagnetic ($J_z > 0$) and antiferromagnetic ($J_z < 0$) coupling for the Ising terms. The latter leads to a rich structure of the ground-state phase diagram as a result of frustration originated from the antiferromagentic interactions on the bonds of triangles (see Fig. 3).

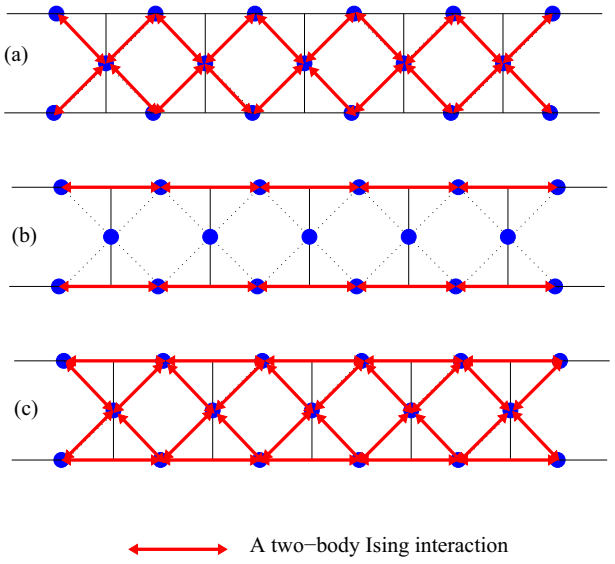

FIG. 2. (Color online) Ising interactions that would be added to the Kitaev ladder. (a) Rhombic-Ising (RI) interactions ($\mathcal{H}_\mathcal{R}$), (b) leg-Ising (LI) interactions ($\mathcal{H}_\mathcal{L}$), and (c) rhombic-leg-Ising (RLI) interactions ($\mathcal{H}_{\mathcal{RL}}$). A two-body Ising interaction $\sigma_i^z\sigma_j^z$ is denoted by $\longleftrightarrow$ between the corresponding spins.

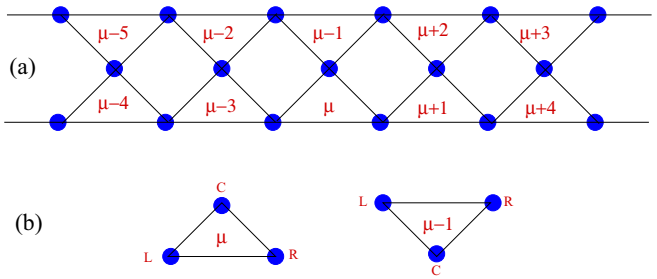

FIG. 3. (Color online) (a) The Kitaev ladder, where each vertex operator (triangle) is denoted as an effective spin (τ^z_μ) labeled by μ. (b) The original spins are relabeled by the triangle index (μ) and its position (L, R, C) on it.

To investigate the competition between the Kitaev and Ising interactions, we consider a Hamiltonian, which is composed of the Kitaev terms in addition to one form of Ising interactions defined in Fig. 2, i.e.,

$$\mathcal{H} = \mathcal{H}_\mathcal{K} + \mathcal{H}_{\text{Ising}}, \tag{6}$$

where $\mathcal{H}_{\text{Ising}}$ is either (A) $\mathcal{H}_\mathcal{R}$, or (B) $\mathcal{H}_\mathcal{L}$ or (C) $\mathcal{H}_{\mathcal{RL}}$. The Hamiltonian is composed of three types of terms, i.e., the vertex (A_v), plaquette (B_p), and Ising ($\sigma^z_i\sigma^z_j$) terms. The plaquette term commutes with both the vertex and Ising ones, $[B_p, A_v] = 0, [B_p, \sigma^z_i\sigma^z_j] = 0$, and consequently does not play any role in the competition for quantum phase transition. However, the plaquette term adds a constant term to the underlying Hamiltonian, which is being fixed to its minimum value for the ground-state properties, i.e., $B_p = +1$.

A. Rhombic-Ising interactions

In this subsection, we consider the competition between Kitaev and rhombic-Ising interactions that is shown in Fig. 2(a) and is given by the following Hamiltonian,

$$\mathcal{H}_{\mathcal{KR}} = \mathcal{H}_\mathcal{K} + \mathcal{H}_\mathcal{R} = -J_v \sum_v A_v + \mathcal{H}_\mathcal{R}, \tag{7}$$

where $\mathcal{H}_\mathcal{R}$ is given by

$$\mathcal{H}_\mathcal{R} = -J_z \sum_\mu \left(\sigma^z_{\mu,C}\sigma^z_{\mu,R} + \sigma^z_{\mu,C}\sigma^z_{\mu,L}\right). \tag{8}$$

The spins are labeled in terms of the notation defined in Fig. 3. In this representation, the spin of the original lattice carries two indices, the label of a triangle (μ) and a label, which sticks to the right (R), left (L) or center (C) of a triangle, as can be seen in Fig. 3(b). Accordingly, a vertex operator is given by

$$A_\mu = \sigma^x_{\mu,L}\sigma^x_{\mu,R}\sigma^x_{\mu,C}. \tag{9}$$

In a qualitative description, we get the Kitaev-SPT phase for $J_z \to 0$, and on the other extreme limit a classical ferromagnetic order for $J_v \to 0$ and $J_z > 0$, which suggests having a quantum phase transition between the mentioned limits. First, we introduce a transformation that gives the effective theory, which illustrates the quantum phase transition of the Kitaev model in the presence of rhombic-Ising interactions. Then, we examine our findings with numerical computations and elaborate the quantum critical properties of the model.

The building block of the effective theory is a triangle that is denoted by a vertex operator. To visualize this picture, the ladder is labeled by its triangles corresponding to each vertex operator as shown in Fig. 3(a). We consider the x representation as the basis of our study. In this representation, a vertex operator (A_μ) has two values either $+1$ or -1, which is denoted by the associated quasispin (τ^z_μ), i.e.,

$$A_\mu \longrightarrow \tau^z_\mu. \tag{10}$$

It concludes that the effect of the Kitaev Hamiltonian on the quasispin representation is like a magnetic field,

$$J_v \sum_v A_v \longrightarrow J_v \sum_\mu \tau^z_\mu. \tag{11}$$

The effect of a single $\sigma^z_{\mu,L}$ on a quasispin (a triangle) is to flip its state, which is denoted by τ^x_μ in the quasispin representation,

$$\sigma^z_{\mu,m} \longrightarrow \tau^x_\mu, \quad m = L, R, C. \tag{12}$$

The rhombic-Ising terms are two-body spin interactions, which act only along the edges of rhombic shapes in Fig. 3(a). It is important to note that an Ising term, which is along an edge of the rhombus does not change the state of a quasispin (a triangle) that shares the mentioned edge. For instance, $\sigma^z_{\mu,C}\sigma^z_{\mu,R}$ flips two times the state of the triangle denoted by μ, which leads to its original state [see Figs. 3(b) and 4]. However, an Ising term, which shares a single spin at the corner of a triangle, flips the associated state of quasispin. In other words, the operation of $\sigma^z_{\mu,C}\sigma^z_{\mu,R}$ flips the state of quasispins (triangles) denoted by $\mu - 1$ and $\mu + 1$ (as shown in Fig. 4). Therefore, each Ising term, like $\sigma^z_{\mu,C}\sigma^z_{\mu,R}$ is represented by the product of two x-component quasispins acting as $\tau^x_{\mu-1}\tau^x_{\mu+1}$,

$$\sigma^z_{\mu,C}\sigma^z_{\mu,R} \longrightarrow \tau^x_{\mu-1}\tau^x_{\mu+1}. \tag{13}$$

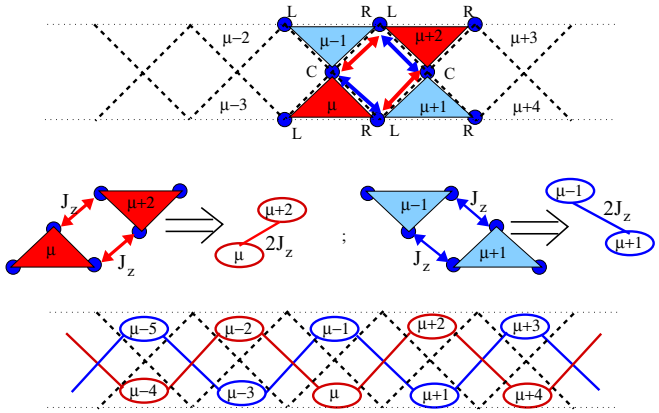

FIG. 4. (Color online) Effective Hamiltonian for the Kitaev ladder with rhombic-Ising interactions. A triangle is considered as a quasispin (τ), which is defined by a vertex operator acting on the corners of a triangle [Eq. (10)]. The Ising interactions, which act only along the edge of rhombuses [see also Fig. 2(a)] changes the state of quasispins (triangles) that are against each other, which is considered as the effective interaction between those quasispins. A quasispin is represented by an oval. Hence, the effective Hamiltonian is composed of two decoupled chains of the transverse field Ising model acting on the quasispin Hilbert space [Eq. (14)].

The Ising interactions on the edges of a rhombus create effective interactions between the quasispins corresponding to the opposite edges. It leads to the effective interaction, $2J_z\tau^x_{\mu-1}\tau^x_{\mu+1}$, between two odd-labeled or two even-labeled quasispins, independently (see Fig. 4). Thus, the effective Hamiltonian ($\mathcal{H}^{\mathcal{R}}_{\rm eff}$), which describes the Kitaev Hamiltonian in the presence of rhombic-Ising interactions, $\mathcal{H}_{\mathcal{K}}+\mathcal{H}_{\mathcal{R}}$, is given by two decoupled chains of the transverse field Ising (TFI) model,

$$\mathcal{H}^{\mathcal{KR}}_{\rm eff} = -2J_z\sum_{\mu}{}' \tau^x_\mu\tau^x_{\mu+2} - J_v\sum_{\mu}{}' \tau^z_\mu, \quad \mu = \text{odd or even}, \tag{14}$$

where $\sum'_\mu$ emphasizes the odd and even quasispins are decoupled. Accordingly, a quantum phase transition takes place exactly at $2J_z = J_v$, which is known from the exact solution of the spin-1/2 TFI chain. Our result is in contrast to $J^c_z = 0$ presented in Ref. [21]. In Ref. [21] the Kitaev ladder with the rhombic-Ising interaction is mapped to a spin-1/2 XY chain using a nonlocal transformation. Their mapping and the effective XY model are correct; however, the conclusion of zero Ising critical coupling ($J^c_z = 0$) overlooks the true QCP. The exactly solvable spin-1/2 XY chain [53] is defined by the Hamiltonian $H_{XY} = J_x\sum_i(s^x_i s^x_{i+1} + \gamma s^y_i s^y_{i+1})$, where $\gamma \equiv J_y/J_x$. For a nonzero value of γ, the XY chain is gapped except at $\gamma = 1$, where the gap vanishes as $|\gamma - 1|$ at momentum $q = \pi/2$. The elementary excitations at the (gapless) critical point are spinons [54]. Moreover, the second derivative of ground-state energy (E_0) diverges as

$$\frac{d^2E_0}{d\gamma^2} \sim |\gamma - 1|^{-3} \quad \text{at} \quad q = \frac{\pi}{2}, \tag{15}$$

which justifies the quantum phase transition at the isotropic point, $\gamma = 1$, that corresponds to our result $J^c_z = J_v/2$.

To gain more insights on the structure of phases and the nature of quantum phase transition, we obtain, using numerical computations, the ground state of the Kitaev ladder in the presence of rhombic-Ising terms using an implementation of the iDMRG algorithm (see Appendix A). The code is based on iMPS representation, where χ denotes the dimension of matrices in this formalism. The entanglement spectrum of the ground state is defined in terms of the eigenvalues of the reduced density matrix. Let ρ be the ground-state reduced density matrix, which is obtained by tracing over half of the ladder from the middle to either the left or right end of the ladder,

$$\rho = tr_{L/2}(|\psi_0\rangle\langle\psi_0|), \tag{16}$$

where $|\psi_0\rangle$ is the ground state of the Kitaev ladder with Ising interactions. Let λ_i be the eigenvalues of ρ; the entanglement spectrum (ES) is defined by $\varepsilon_i = -\ln(\lambda_i)$. We have plotted the entanglement spectrum versus J_z of the Kitaev ladder in the presence of rhombic-Ising interactions in Fig. 5, which exhibits a change of degeneracy at $J_z = 0.5$. We set $J_v = 1$ as the scale of energy in all plots and results unless it appears explicitly. The spectrum has even degeneracy for $0 \leqslant J_z < 0.5$, which is a clear signature for the SPT character of the Kitaev phase, while it has mixed degeneracy for $J_z > 0.5$ in the (trivial) ferromagnetic product state. The change of degeneracy of the entanglement spectrum at $J_z = 0.5$ is an indication of the quantum phase transition, which is accompanied by a qualitative change in the ground state.

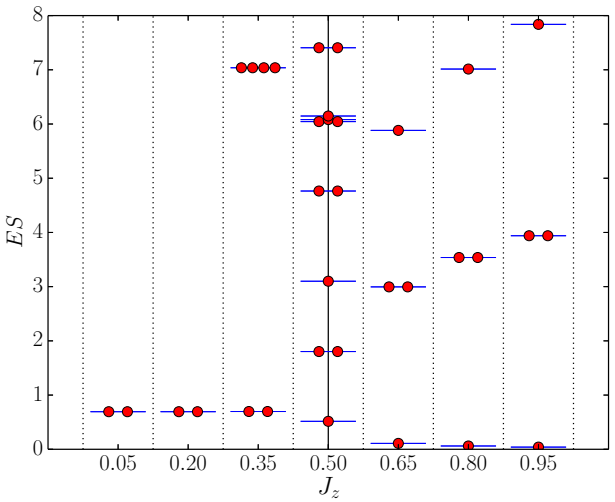

FIG. 5. (Color online) Entanglement spectrum (ES) versus J_z for the ground state of $\mathcal{H}_{\mathcal{K}} + \mathcal{H}_{\mathcal{R}}$. The lowest level is doubly degenerate for $0 \leqslant J_z < 0.5$, which is a signature of SPT character, while it is nondegenerate for $J_z > 0.5$ in the (trivial) ferromagnetic product state. At the quantum critical point $J_z = 0.5$, the spectrum becomes dispersed over the entire range of eigenvalues, which is a signature of the critical point.

The von-Neumann (entanglement) entropy (S_E) is defined in terms of the eigenvalues of ρ,

$$S_E = -\sum_i \lambda_i \ln(\lambda_i). \tag{17}$$

We have plotted S_E versus J_z in Fig. 6 for different $\chi = 8, 16, 32, 64$. The entropy shows a divergent behavior only at $J_z = 0.5$, which justifies the quantum phase transition. As shown in Fig. 6, S_E asymptotically reaches the value of ln(2) for the pure Kitaev ladder ($J_z = 0$), which is the signature

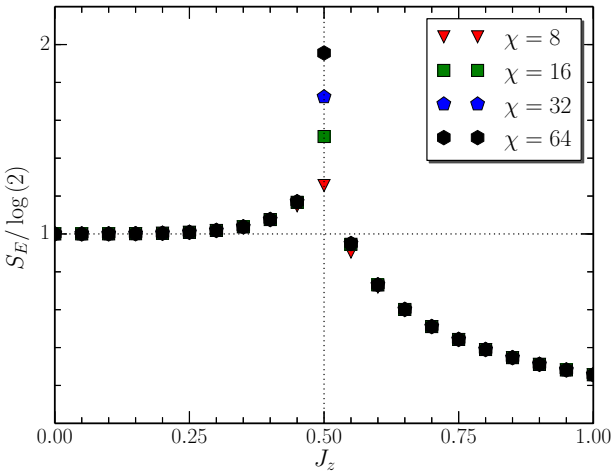

FIG. 6. (Color online) von-Neumann entropy (S_E) versus J_z for Kitaev plus rhombic-Ising interactions. The divergent behavior of S_E at $J_z = 0.5$ is a clear signature of quantum phase transition. S_E reaches ln(2) asymptotically for the pure Kitaev ladder ($J_z = 0$).

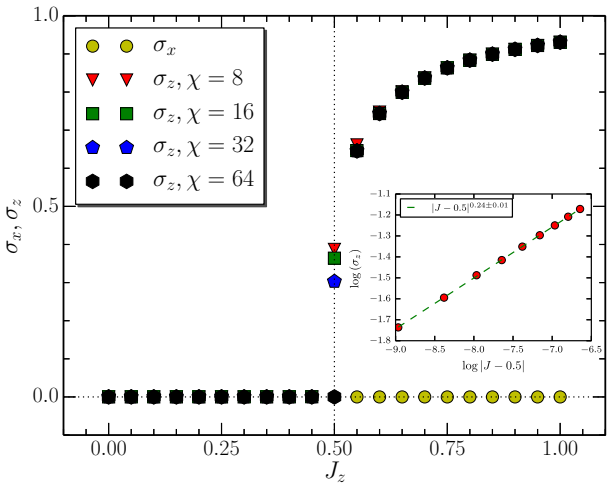

FIG. 7. (Color online) Magnetic order parameters versus J_z for Kitaev plus RI interactions. The ferromagnetic order parameter $\langle\sigma_z\rangle$ becomes nonzero for $J_z \geqslant 0.5$ justifying the quantum phase transition to the symmetry-broken state. The inset shows the scaling of $\langle\sigma_z\rangle \sim (J-0.5)^{(0.24\pm0.01)}$, where the horizontal axis is in log scale, close to the critical point.

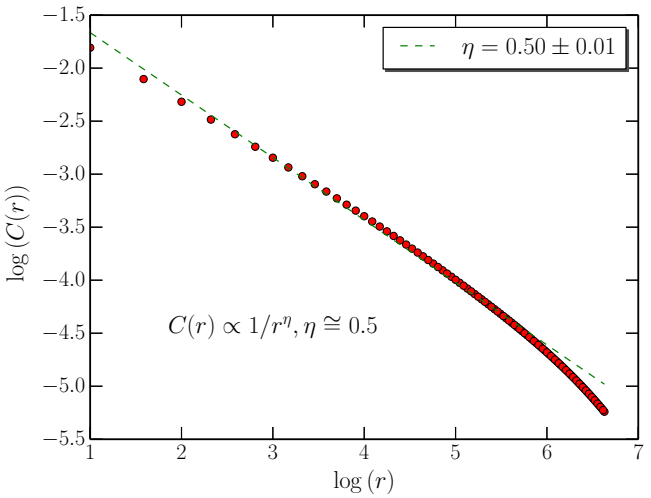

FIG. 8. (Color online) Log-log plot of correlation function $C(r)$ versus r for the Kitaev-rhombic-Ising ladder at the QCP. The (green) dotted line shows the best fit of $r^{(-0.5)}$, which states $\eta = 0.50 \pm 0.01$. The correlation length is $\xi \backsimeq 400$ for $\chi = 150$, which determines the reliable behavior for $r < \xi$, i.e., $\log(r) \lesssim 5.99$.

of its SPT character (the double degeneracy of ES), while it vanishes in the extreme Ising limit ($J_z \to \infty$) representing a product state of up (or down) spins in a ferromagnetic state.

We have also computed the ordinary magnetic order parameter on both sides of the quantum critical point. We have plotted in Fig. 7 the magnetic order parameters in the x and z directions, $\langle\sigma_x\rangle$ and $\langle\sigma_z\rangle$, respectively. $\langle\sigma_x\rangle$ is always zero for the whole range of J_z, which shows no magnetic order in the x direction. However, $\langle\sigma_z\rangle$ becomes nonzero at $J_z = 0.5$ indicating the magnetic order of the ferromagnetic state. Approaching the quantum critical point from the ferromagnetic phase ($J_z > 0.5$) shows $\langle\sigma_z\rangle$ to vanish like $(J-0.5)^{(0.24\pm0.01)}$ manifesting a second-order phase transition with exponent $\beta = 0.24 \pm 0.01$ (the inset of Fig. 7), in agreement with the effective theory described in Eq. (14). The effective theory, for the Kitaev ladder with rhombic-Ising interactions, is expressed in terms of two decoupled TFI chains, which predicts the central charge for the corresponding QPT at $J_z = 0.5$ is being twice the central charge of the TFI chain, i.e., $c = 2 \times 0.5 = 1$. Similar argument shows that the magnetization exponent, which comes out of the effective theory, is $\beta = 1/4$, which is elaborated in the following.

The ferromagnetic order parameter $\langle\sigma_z\rangle$ is

$$\langle\sigma_z\rangle = \frac{1}{3N}\sum_{\mu=1}^{N}\langle\psi_0|\left(\sigma^z_{\mu,C} + \sigma^z_{\mu,R} + \sigma^z_{\mu,L}\right)|\psi_0\rangle. \tag{18}$$

The effect of $\sigma^z_{\mu,C}$ on the ground state of the ladder ($|\psi_0\rangle$) is equivalent to flipping the state of the quasispins denoted by the two triangles, which share $\sigma^z_{\mu,C}$ at their common corner (see Fig. 3). It is shown by

$$\sigma^z_{\mu,C}|\psi_0\rangle = \tau^x_{\mu}\left|\varphi_0^{(\text{even})}\right\rangle \otimes \tau^x_{\mu-1}\left|\varphi_0^{(\text{odd})}\right\rangle, \tag{19}$$

where $|\varphi_0^{(\text{even})}\rangle$ ($|\varphi_0^{(\text{odd})}\rangle$) represents the ground state of TFI effective theory for the even (odd) decoupled chain. Hence, we conclude that

$$\langle\sigma_z\rangle = (\langle\tau^x\rangle_{\text{TFI}})^2 = \left|J_z - J_z^c\right|^{\frac{1}{4}}, \tag{20}$$

which leads to $\beta = 1/4$ as confirmed numerically in the inset of Fig. 7. A similar calculation gives the exponent of the algebraic decay of correlation functions at the QCP,

$$C(r)|_{J_z=J_z^c} = \left\langle\sigma^z_1(i)\sigma^z_1(i+r)\right\rangle \sim \frac{1}{r^{\eta}}, \qquad \eta = \frac{1}{2}, \tag{21}$$

where $\sigma^z_1(i)$ is defined in a unit cell of Fig. 1. This is in agreement with the numerical computation of correlation function of the Kitaev RI ladder performed at $J_z = J_z^c = 0.5$ in Fig. 8, where the numerical exponent is $\eta = 0.50 \pm 0.01$. It should be noticed that both β and η exponents are twice the corresponding one of the TFI chain. It means that the decoupled chains of the effective theory contribute to the quantum critical properties of the original ladder. In other words, although the effective TFI chains are decoupled they are not independent.

Moreover, we have numerically calculated the central charge at the critical point $J_z = 0.5$, which leads to $c = 1.01 \pm 0.01$ as shown in Fig. 9(a). The central charge is calculated within finite-entanglement scaling introduced in Refs. [55–57]. In this approach, the scaling of S_E with the correlation length (ξ) would give a fair approximation of the central charge (see Appendix A). The numerical result confirms that the effective theory truly captures the critical properties of the original model.

We have plotted the phase factor order parameter $\mathcal{O}$ versus J_z in Fig. 10. It shows that for small values of $J_z < J_z^c$, the model is in the SPT phase of the Kitaev ladder, which is justified by $\mathcal{O} = -1$. More specifically, Fig. 10(a) shows that for $J_z < 0.5$ the model represents an SPT phase, while it shows a symmetry-broken trivial phase ($\mathcal{O} = 0$) for $J_z > 0.5$ via a quantum phase transition. The symmetry-broken phase does

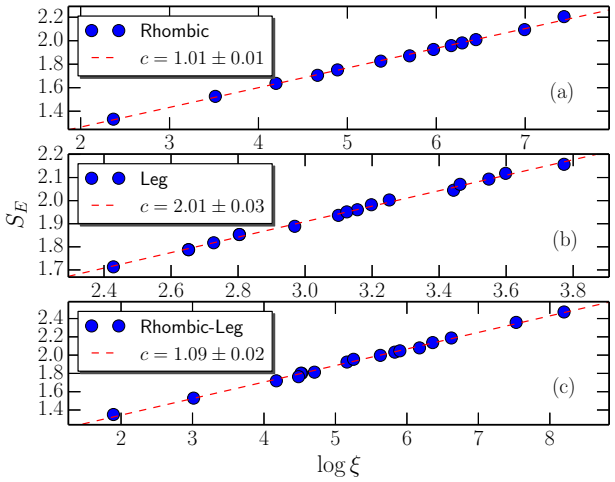

FIG. 9. (Color online) S_E versus $\log(\xi)$, which gives the central charge of the Kitaev ladder in addition to (a) RI, (b) LI, and (c) RLI interactions according to the finite entanglement scaling (see Appendix A and Refs. [55–57]).

not respect the symmetry, which gives the largest eigenvalue of the transfer matrix to be less than 1, leading to $\mathcal{O} = 0$.

Almost the whole discussion of the ferromagnetic rhombic-Ising interaction is also valid for the antiferromagnetic Ising interaction. In other words, we can simply consider a mirror image of all Figs. 5, 6, 7, and 10 with respect to $J_z = 0$ to get the antiferromagnetic regime. A better understanding can be achieved by considering a π rotation around the x axis for the spins sitting on the rungs of the ladder and $J_z \to -J_z$, which leaves the whole Hamiltonian invariant.

B. Leg-Ising interactions

The Ising terms may be considered only between the spins on the legs of the ladder, without any inter-leg interaction; see Fig. 2. Therefore, the Ising interactions would be between spins labeled L and R, namely, $\sigma^z_{\mu,R}\sigma^z_{\mu,L}$, which is given by

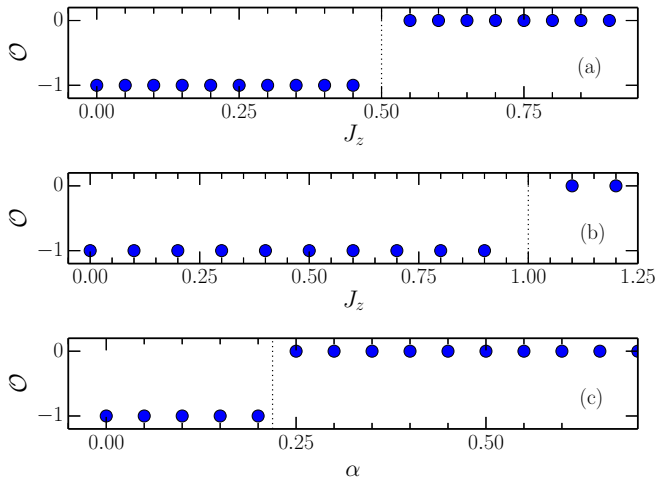

FIG. 10. (Color online) Phase factor order parameter for the ferromagnetic Kitaev ladder in the presence of (a) RI, (b) LI, and (c) RLI interactions.

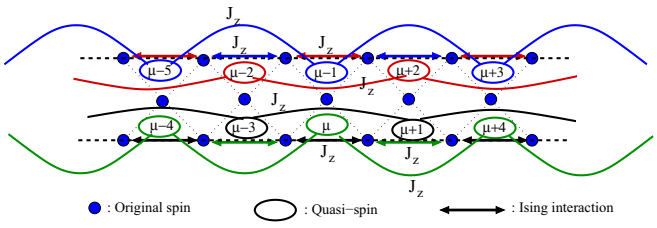

FIG. 11. (Color online) Effective Hamiltonian for the Kitaev ladder with leg-Ising interactions. An Ising interacting along the leg of the original ladder is shown with $\longleftrightarrow$, which acts on the original spins. Different colors of $\longleftrightarrow$ lead to effective interactions between quasispins, represented by an oval of the same color. Accordingly, the effective Hamiltonian is equivalent to four decoupled TFI chains acting on quasispins of different colors, denoted by tick-colored lines.

the following Hamiltonian:

$$\mathcal{H}_{\mathcal{L}} = -J_z \sum_{\mu} \sigma^z_{\mu,L}\sigma^z_{\mu,R}. \tag{22}$$

We explain the effect of $\sigma^z_{\mu,R}\sigma^z_{\mu,L}$ on quasispins. The quasispin associated with μ is not changed by this Ising term as it flips two original spins, which leaves the product of spins on the triangle (quasispin) unchanged. However, the quasispins labeled $\mu - 3$ and $\mu + 1$ are being flipped (see Fig. 11), which initiates the following correspondence in terms of quasispin operators,

$$\sigma^z_{\mu,R}\sigma^z_{\mu,L} \longrightarrow \tau^x_{\mu-3}\tau^x_{\mu+1}. \tag{23}$$

In accordance with Eq. (23), the Ising interactions along the legs are responsible for the interactions between the quasispins labeled mod(4, n), independently, where $n = 0, 1, 2, 3$. Therefore, the effective Hamiltonian is described by four decoupled TFI chains, namely,

$$\mathcal{H}^{\mathcal{KL}}_{\text{eff}} = -J_z \sum_{\mu}'' \tau^x_{\mu}\tau^x_{\mu+4} - J_v \sum_{\mu}'' \tau^z_{\mu}, \tag{24}$$

where $\sum''_{\mu}$ indicates four decoupled chains as shown in Fig. 11. The effective model shows a quantum phase transition at $J_z = J_v$.

The quantum phase transition at $J_z = 1$ (for $J_v = 1$) is justified by von-Neumann entropy versus J_z plotted in Fig. 12. For the small Ising coupling ($J_z \to 0$) S_E is equal to ln(2) confirming the SPT phase of the pure Kitaev ladder. The entropy rises up and becomes divergent at $J_z = 1$, which is the signature of the quantum phase transition. Increasing the value of $J_z > 1$ leads to a ferromagnetic phase for the original spins ordered in the z direction and mediated by the Ising interactions along the legs of the ladder. The factorized ferromagnetic state gives a zero value for S_E as is shown in Fig. 12 for the strong Ising coupling ($J_z \to \infty$).

Another indication of the quantum phase transition is found in the structure of the entanglement spectrum and especially the degeneracy of levels. The degeneracy of the entanglement spectrum is even for $J_z < 1$ while it has mixed degeneracy for $J_z > 1$ (not shown here). The type of spectrum is similar to Fig. 5 except the change of degeneracy, which occurs at $J_z = 1$. The even degeneracy for $J_z < 1$ is a signature of the

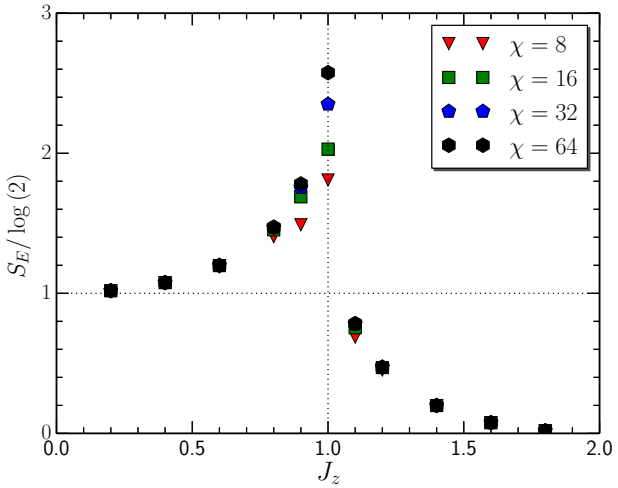

FIG. 12. (Color online) von-Neumann entropy versus J_z for the Kitaev ladder with leg-Ising interactions. The entropy diverges exactly at $J_z = 1$ confirmed by the effective theory ($\mathcal{H}_{\text{eff}}^{\mathcal{KL}}$).

Kitaev SPT phase, which is verified by $\mathcal{O} = -1$ in Fig. 10(b). The phase factor order parameter ($\mathcal{O}$) jumps to zero for $J_z > 1$.

Our numerical results show that the quantum critical point between Kitaev SPT and the ferromagnetic leg-Ising phase is described by the central charge $c = 2.01 \pm 0.03$ as shown in Fig. 9(b). This is in agreement with the effective theory obtained in Eq. (24), which shows four decoupled TFI chains that give $c = 4 \times 0.5 = 2$.

The phase diagram of the Kitaev ladder with the antiferromagnetic leg-Ising interaction is the mirror image of the ferromagentic phase diagram with respect to $J_z = 0$. In fact, the full Hamiltonian is invariant under the transformation $J_z \to -J_z$ and a π rotation around the x axis on the even (or odd) spins on the legs of the ladder.

C. Rhombic-leg-Ising interactions

Here, we consider the Ising interactions along both the legs and the rhombic plaquettes [shown in Fig. 2(c)] that leads to a very interesting phase diagram, where the full Hamiltonian is given by

$$\mathcal{H}_{\mathcal{KRL}} = (1 - |\alpha|)\mathcal{H}_{\mathcal{K}} + \alpha(\mathcal{H}_{\mathcal{R}} + \mathcal{H}_{\mathcal{L}}), \quad |\alpha| \leqslant 1. \tag{25}$$

Here, we introduce α to sweep between the extreme limits of the Kitaev interaction for $\alpha = 0$ and the Ising limit for $|\alpha| = 1$. $\alpha > 0$ corresponds to the ferromagnetic Ising interactions, while $\alpha < 0$ represents the antiferromagnetic ones. The ground-state phase diagram can be understood in terms of competition between the nearest- and next-nearest neighbor interactions, which come out of the effective theory. The antiferromagnetic Ising interactions have specific features, where frustration hinders simultaneous minimization of energy according to a classical antiferromagnetic state. The effective theory is simply obtained by incorporating the representation of rhombic-Ising (Fig. 4) and leg-Ising (Fig. 11) interactions in the quasispin representations. The Ising terms on rhombuses lead to Ising interactions between even (odd) quasispins, while the leg terms establish interactions between quasispins of μ and $\mu + 4$. Hence, the even and odd chain of quasispins remain decoupled bearing the next-nearest-neighbor interactions, which are the effect of leg-Ising interactions. This can be seen in Fig. 13, where solid red (blue) lines show NN and dashed red (blue) lines represent NNN interactions for the even (odd) decoupled effective chains. It should be mentioned that the strength of NNN coupling is half the NN one. The effective Hamiltonian for the Kitaev ladder in the presence of rhombic-leg-Ising interactions is given by

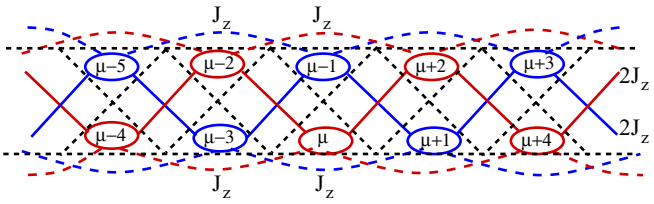

FIG. 13. (Color online) The effective interactions between the quasispins for the Kitaev ladder with both rhombic- and leg-Ising terms. The rhombic terms create two decoupled TFI chains, namely odd and even ones, where the leg terms add the next-nearest-neighbor interactions on each chain, separately. Solid red (blue) lines represent the nearest-neighbor interactions, while dashed red (blue) lines show the next-nearest-neighbor ones, on even (odd) quasispins.

$$\mathcal{H}_{\text{eff}}^{\mathcal{KRL}} = -\alpha J_z \sum_{\mu}{}' \left(2\tau_{\mu}^{x}\tau_{\mu+2}^{x} + \tau_{\mu}^{x}\tau_{\mu+4}^{x}\right) - (1 - |\alpha|)J_v \sum_{\mu}{}' \tau_{\mu}^{z}, \quad \mu = \text{odd or even}. \tag{26}$$

The presence of NNN interactions in the antiferromagnetic regime leads to interesting and exotic features in the model. Thus, we discuss the ferromagnetic and antiferromagnetic cases in the following two subsections, separately.

1. Ferromagnetic RL Ising

Contrary to the RI and LI cases, the effective theory for the Kitaev ladder in the presence of both the leg- and rhombic-Ising terms does not have an exact solution due to the NNN coupling in the TFI effective chain. Our numerical simulation of entropy, S_E versus α is plotted in Fig. 14, which shows divergent behavior at the critical point $\alpha_c^{\mathcal{KRL}} = 0.219 \pm 0.001$. This is equivalent to a phase transition at $(J_z/J_v) = 0.280 \pm 0.001$ with a rescaling of the Kitaev and Ising couplings in Eq. (25). Here, the presence of Ising interactions on all bonds (legs and rhombuses) sustain the ferromagnetic order to overcome the Kitaev SPT phase within smaller J_z coupling than the RI and LI cases. The model represents the Kitaev SPT phase for $\alpha < \alpha_c^{\mathcal{KRL}}$, with finite entanglement entropy ln(2), double degeneracy in the entanglement spectrum, no (local) magnetic order, and phase factor order parameter $\mathcal{O} = -1$ in Fig. 10(c). A second-order phase transition drives the model to the (trivial) ferromagnetic phase for $\alpha > \alpha_c^{\mathcal{KRL}}$, which is presented by a factorized state of up (or down) spins in the z direction. The quantum critical point is described by the central charge $c = 2 \times 0.5 = 1$ given by two decoupled NNN TFI chains and justified by numerical simulation in Fig. 9(c), which renders $c = 1.09 \pm 0.02$.

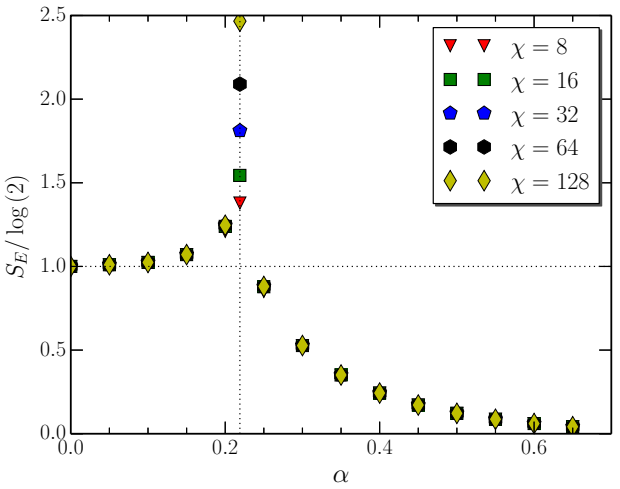

FIG. 14. (Color online) von-Neumann entropy [scaled by ln(2)] versus α for the Kitaev ladder in the presence of ferromagnetic rhombic-leg-Ising interactions.

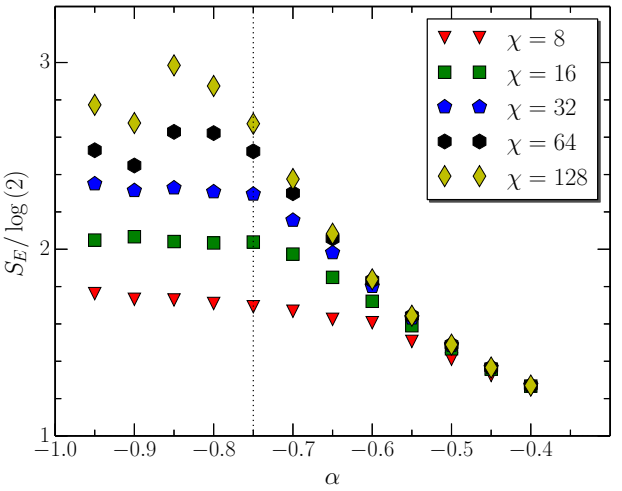

FIG. 16. (Color online) von-Neumann entropy versus α for the Kitaev ladder in the presence of AF RL-Ising interactions.

2. *Antiferromagnetic RL Ising*

The antiferromagnetic Ising interactions on both legs and rhombus bonds create the basic building block of frustrated magnetic systems, i.e., triangles with antiferromagnetic bonds [see Fig. 2(c)]. The antiferromagnetic Hamiltonian is defined by Eq. (25) with $-1 \leqslant \alpha \leqslant 0$. Although the ground state of the model is twofold degenerate at the Kitaev limit ($\alpha = 0$) it has exponentially degenerate ground-state configurations at the AF Ising limit ($\alpha = -1$). To get more insight on the model at the AF Ising limit, we associate a magnetization (m^z_μ) with each triangle, which is simply the total magnetization in the z direction of a single triangle. For the ground state, the antiferromagnetic nature of interactions forces the spins on each triangle to be oriented as either 2-up-1-down or 2-down-1-up (see Fig. 15), which yields $m^z_\mu = \pm 1$. Therefore,

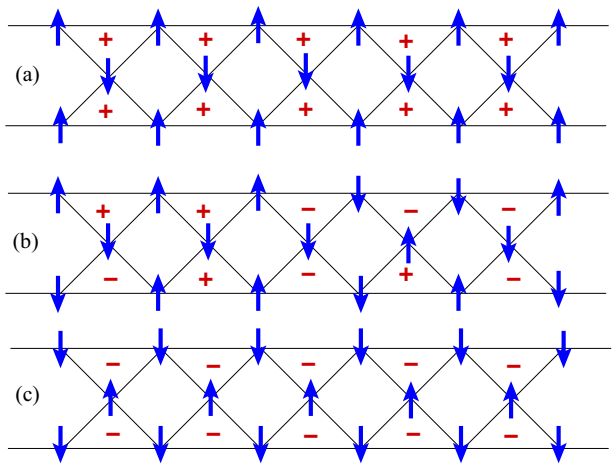

FIG. 15. (Color online) Some of the ground-state configurations at the antiferromagnetic rhombic-leg-Ising limit ($J_v = 0$) of the two-leg ladder. The $\uparrow$ and $\downarrow$ represent σ^z spin orientation. The $\pm$ shows the sum of σ^z spins in each triangle. All configurations are classified as 2-up-1-down or 2-down-1-up for each triangle.

the ground-state degeneracy at the AF Ising limit is 2^{2N}, where $2N$ is the number of triangles in the ladder (assuming a periodic boundary condition along the legs). The spins that sit on the legs of the ladder are not constrained to a boundary condition perpendicular to the legs of the ladder, which leads to an intensive degenerate configuration with total magnetization $M^z \in \{2N, 2N-1, \ldots, -2N+1, -2N\}$,

$$M^z = \sum_{\mu=1}^{2N} m^z_\mu. \tag{27}$$

Some configurations of the mentioned subspace are shown in Fig. 15, where the $\pm$ in each triangle represents m^z_μ. A state with $M^z = 2N$ is shown in Fig. 15(a), where all triangles carry $m^z_\mu = +$; an intermediate state with $M^z = 0$ is presented in Fig. 15(b) and a state of all $m^z_\mu = -$ is given in Fig. 15(c). Accordingly, the model does not show a magnetic long-range order out of a symmetry breaking, which is called a *classical spin liquid*. A classical spin-liquid state shows no long-range order, an extensive degeneracy of ground state and algebraic decay of correlation functions.

We have plotted S_E versus α in Fig. 16 for the Kitaev ladder in the presence of AF RL-Ising interactions. Our data shows that S_E reaches ln(2) for $\alpha \to 0$, which is the signature of the Kitaev SPT phase. The entanglement entropy shows finite entanglement scaling for $-1 < \alpha < -0.7$, which is represented by $\chi = 8, 16, 32, 64, 128$. Although a bump is observed around $\alpha \simeq -0.8$ the whole set of data does not conclude to a single divergent peak, rather showing a broad area of finite entanglement scaling. It suggests a broad critical area, which starts at $\alpha = -1$ (the classical spin liquid) toward an intermediate region, $\alpha \simeq -0.75$, where the Kitaev SPT phase dominates. This is confirmed by the structure of the entanglement spectrum versus α presented in Fig. 17. We have shown in Sec. II that the ground state of the Kitaev ladder is an SPT phase, which leads to even degeneracy of ES. Accordingly, the even degeneracy of ES is the signature of the Kitaev SPT phase for $\alpha_c < \alpha \leqslant 0$, where $\alpha_c = -0.75 \pm 0.05$. The computation for higher values of χ (> 128) is a massive

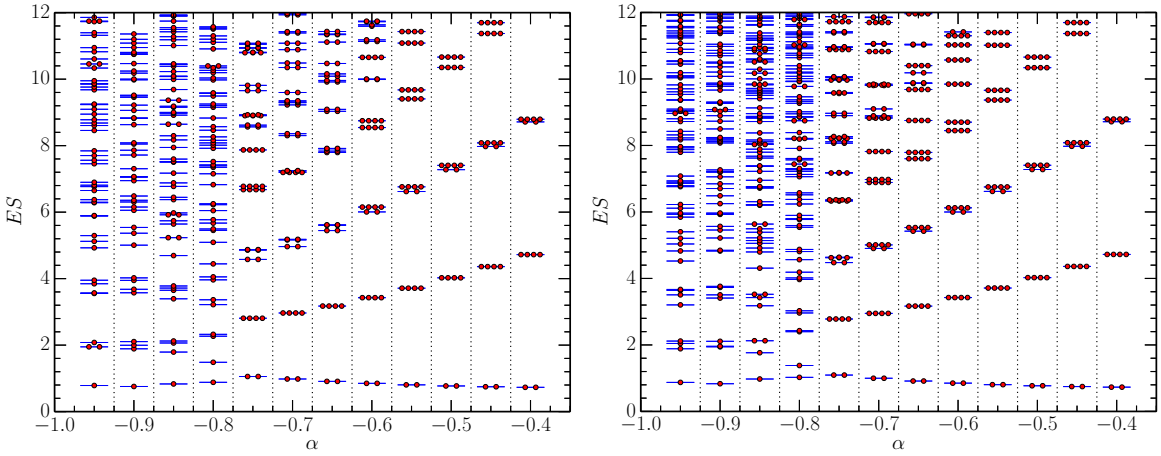

FIG. 17. (Color online) Entanglement spectrum versus α for the Kitaev ladder in the presence of AF RL-Ising interactions. (Left) $\chi = 64$, (right) $\chi = 128$.

time consumption for our model, where the unit cell contains three spin-1/2. However, the results shown in Fig. 17 for $\chi = 64$ (left), $\chi = 128$ (right), and other $\chi = 16,32$ (not shown here) convince us that the degeneracy of Kitaev SPT is persistent for $\alpha_c < \alpha \leqslant 0$. For $-1 < \alpha \leqslant \alpha_c$, the model shows finite entanglement scaling (Fig. 16) and dispersed ES (Fig. 17), which resembles a critical area with algebraic decay of correlation functions. This is consistent with the conclusion that can be derived from the effective theory.

The effective Hamiltonian defined in Eq. (26) for the Kitaev ladder in the presence of AF RL-Ising interactions renders the frustrated NNN TFI chain in which the NNN coupling is half of the NN coupling, being denoted by $\kappa = 0.5$. The effective theory at $\alpha = -1$ falls exactly on the critical point $\kappa = 0.5$ at the zero transverse field, which separates the antiferromagnetic phase from the antiphase of frustrated NNN TFI [37,40,41,43]. It states that the classical spin liquid of the AF RL-Ising limit corresponds to the critical point of the frustrated NNN TFI model at the zero transverse field. The onset of the Kitaev term ($\alpha \neq -1$) adds quantum fluctuations to the model, which corresponds to the effect of the transverse field on the frustrated NNN TFI critical point. A recent study on the frustrated NNN TFI chain [43] confirms the existence of a tri-critical point at $\kappa = 0.5$, where a Kosterlitz-Thouless transition line and two second-order transition lines merge at $\kappa = 0.5$ and zero field. Thus, the effect of the Kitaev term on the classical spin liquid is similar to the effect of the transverse field on frustrated NNN TFI at $\kappa = 0.5$ toward passing through the floating phase before reaching a paramagnetic phase. The floating phase has algebraic decaying correlation functions, which could lead to finite entanglement scaling and broad dispersion of ES. Therefore, our results in Figs. 16 and 17 are in agreement with the phase diagram proposed in Refs. [41,42] for NNN TFI (that is sometimes denoted by the ANNNI model in the literature).

IV. SUMMARY AND DISCUSSION

We have studied the Kitaev Hamiltonian ($\mathcal{H}_\mathcal{K}$) on a ladder geometry. We find that the ground state of the Kitaev ladder is an SPT phase protected by $\mathbb{Z}_2 \times \mathbb{Z}_2$ symmetries namely $\mathcal{X} = \prod_i \sigma_i^x$ which runs over all ladder bonds and $\mathcal{Z} = \prod_{\ell \notin \text{rungs}} \sigma_\ell^z$ that excludes the rung bonds. We have justified our argument by employing the iDMRG method within an iMPS representation, which leads to an inequivalent projective representation of $\mathbb{Z}_2 \times \mathbb{Z}_2$ symmetries providing the phase factor order parameter $\mathcal{O} = -1$, for the Kitaev phase.

We have also investigated the competition between the Kitaev and Ising terms on the ladder, which is given by deriving the corresponding effective theory in addition to the direct iDMRG computations. For the Ising interactions being solely on the edges of the rhombus or on the legs, the effective Hamiltonian is given by decoupled one-dimensional TFI models, which explains the quantum phase transition from the Kitaev SPT phase to the antiferro/ferromagnetic phase at the exact finite value $J_z/J_v = 0.5,1.0$, respectively. The quantum phase transition is justified by numerical divergence of entanglement entropy (S_E) at the critical point, the change in the degeneracy of the entanglement spectrum, and magnetic order parameters. The quantum critical points and their corresponding central charges of the effective theory and iDMRG results agree with each other, exactly. The critical behavior of Kitaev-rhombic-Ising interactions is given by central charge $c = 1$, while the Kitaev-leg-Ising ladder is represented by $c = 2$. If the Ising interactions reside on both the rhombus and legs of the ladder, the effective theory would be NNN TFI chain with the critical properties given by $c = 1$. For the ferromagnetic Ising interactions it leads to a quantum phase transition at finite ratio $J_z/J_v = 0.280 \pm 0.001$, while for the antiferromagnetic Ising interactions our data show a broad range of finite entanglement scaling. It is the interplay between the classical spin liquid at the AF Ising limit and the Kitaev SPT phases. According to the effective theory, the onset of the Kitaev term induces quantum fluctuations in the classical spin-liquid subspace, which would finally lead to the Kitaev SPT phase passing through an intermediate floating phase. The Kitaev SPT phase is persistent for $|J_z|/J_v \lesssim 3$ witnessed by the even degeneracy of the entanglement spectrum.

The phase diagram of the Kitaev ladder in the presence of mentioned Ising interactions is plotted in Fig. 18. Moreover, the quantum critical properties and the effective theory of each case are summarized in Table I.

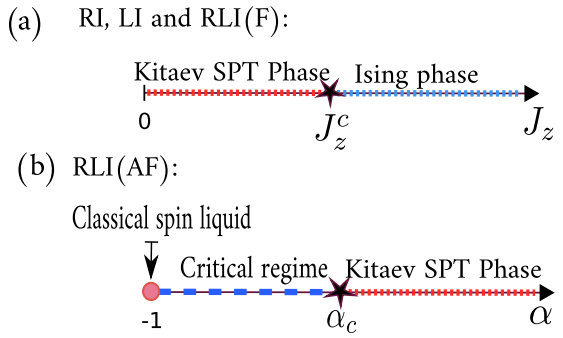

FIG. 18. (Color online) Phase diagram of the Kitaev ladder with Ising interactions. (a) The case of ferro/antiferromagnetic RI or LI and ferromagnetic RLI interactions. (b) Antiferromagnetic RLI interactions, where $\frac{\alpha}{1-|\alpha|} = \frac{J_z}{J_v}$.

A remark is in order concerning the effective theory introduced in this paper. For simplicity, we consider the ladder geometry with a periodic boundary condition along the legs, where N is the number of spins sitting on each leg or rung of ladder, which sums up to $3N$ spins. The dimension of the Hilbert space of the original ladder is 2^{3N}. The number of triangles (quasispins) is $2N$ and the number of rhombuses (plaquettes) is N. Accordingly, the dimension of the Hilbert space of the effective theory (in terms of quasispins) is 2^{2N} which is smaller than the original Hilbert space by a factor of 2^N. In principle, this is always the case for an effective theory, which is responsible for the low-energy behavior of the original model and is confirmed by numerical iDMRG results. However, taking into account the plaquette degrees of freedom ($B_p = \pm 1$) we find the lost 2^N degrees of freedom. For the lowest energy spectrum we consider all N plaquettes to be at $B_p = +1$, which adds a constant term $-J_p N$ to the effective theory. As far as all configurations of the original spin model have been kept in constructing the effective theory we expect that the whole spectrum of the original model is represented by a tower of TFI models in addition to their corresponding constant values, i.e., $(-J_p)\sum_p B_p$. Having in mind that the effective theory considers the whole degrees of freedom of the original model, we have found the exact critical exponents of the mentioned QCPs, summarized in Table I in agreement with the numerical simulations.

The extension of our approach to the two-dimensional case would lead to study the competition between the topological $\mathbb{Z}_2$ spin-liquid state of the toric code with the symmetry-broken or classical spin-liquid state of Ising interactions. A special case has been studied in Ref. [21], which gives the two-dimensional transverse field Ising model as the effective Hamiltonian. A straightforward extension of our effective model would give the two-dimensional TFI model for different configurations of Ising interactions, which will be elaborated on in future works.

Our approach can also be applied to the Kitaev (honeycomb) model on ladder geometry. The model has been investigated in Refs. [45–47], which shows topological phases that have been characterized by string order parameters. One may investigate the nature of topological phases, using our approach—symmetry fractionalization and finite-entanglement scaling— to get more information about these phases.

TABLE I. A summary of quantum critical properties of the Kitaev ladder with Ising interactions defined in Fig. 2. J_z^c is the quantum critical point (assuming $J_v = 1$), c is the central charge, β is the magnetization critical exponent, and η is the correlation function exponent.

Model	J_z^c	c	β	η	Effective theory
RI	0.5	1	1/4	1/2	Two decoupled TFI chains
LI	1	2	1/4	1/2	Four decoupled TFI chains
RLI(F)	0.280	1	1/4	1/2	Two decoupled NNN TFI chains

ACKNOWLEDGMENTS

The authors would like to thank S. Bhattacharjee, M. Kargarian, J. Kjäll, S. Moghimi-Araghi, O. Petrova, F. Pollmann, and A. T. Rezakhani for fruitful discussions and comments. This work was supported in part by the Office of Vice President for Research of Sharif University of Technology. A.L. gratefully acknowledges the Alexander von Humboldt Foundation for financial support.

APPENDIX A: NUMERICAL APPROACH: iDMRG

To examine the properties of the model, we have made use of the standard iDRMG technique that is based on an infinite matrix product state (iMPS) representation for the ground state [48,50]. It is a well-known fact that iMPS is an efficient method to describe translationally invariant many-body states with an accuracy depending on the dimension of implemented matrices [58,59].

The translationally invariant ground state is characterized by canonical [60] Γ and Λ matrices,

$$|\Psi\rangle = \sum_{s_1,\ldots,s_N} \mathrm{Tr}[\Gamma^{s_1}\Lambda \ldots \Gamma^{s_N}\Lambda]|s_1 \ldots s_N\rangle, \tag{A1}$$

which satisfy the following (fixed point) relation,

$$\sum_s \Gamma^s \Lambda^s \Lambda^{s\dagger}\Gamma^{s\dagger} = \mathbb{1}, \tag{A2}$$

where the sum is over different spin configurations and Γs serve as the matrix coefficients for these configurations.

The spectrum (i.e., singular values in the Schmidt decomposition of the left and right bipartition of the Hilbert space) is simply the square root of Λ and the entanglement entropy is defined as

$$S_{\mathrm{E}} = -\sum_i \Lambda_{ii}^2 \log\left(\Lambda_{ii}^2\right). \tag{A3}$$

In the general case, to give an exact representation of a state, iDMRG needs infinitely large matrices. Hopefully, this is not necessary, especially in the case of gapped systems, by putting an upper bound on the cardinality of the matrices χ, and truncating the spectrum, one can reach a good approximation, which has all the properties of the low-energy state. This will give rise to the so-called truncation error which can be

controlled by the dimension of matrices and is the cause of the entropy scaling.

Since the ground state is known to be gapped for the extreme coupling limit of our model, it can be represented by a finite iMPS, where the truncation error for the couplings that are far from the critical point, is less than machine precision. However, close to the critical point, when the ground-state entanglement spectrum should show a long tail, the truncation errors become considerable and they do not vanish even when we increase the size of the matrices.

After reaching the canonical Λ, Γ with the desired accuracy, several properties of the ground state can be evaluated using the iMPS representation. It includes any local observable like energy and σ^z, entanglement spectrum and the corresponding von-Neumann entropy, the application of symmetry operators, and the ground-state fidelity [61]. In order to calculate the mentioned quantities the concept of the transfer matrix should be introduced:

$$T_{\alpha\alpha',\beta\beta'} = \sum_s \left(\Gamma^s_{\alpha\beta}\Lambda_\beta\right)\left(\Gamma^s_{\alpha'\beta'}\Lambda_{\beta'}\right)^*. \tag{A4}$$

The expectation value of a local operator (defined on one specific site), such as $\hat{\mathcal{O}}$, is obtained by using the following transfer matrix:

$$\widehat{T}_{\alpha\alpha',\beta\beta'} = \sum_{s,s'} \left(\Gamma^s_{\alpha\beta}\Lambda_\beta\right)\hat{\mathcal{O}}^{s,s'}\left(\Gamma^{s'}_{\alpha'\beta'}\Lambda_{\beta'}\right)^*. \tag{A5}$$

The expectation value of $\langle\Psi|\hat{\mathcal{O}}|\Psi\rangle$ simply reduces to $\mathrm{Tr}(\Lambda \otimes \Lambda\widehat{T})$. The central charge is calculated according to the scaling relation between von-Neumann entropy and the correlation length. The correlation length is defined as the second largest eigenvalue (e_2) of the transfer matrix T [55–57,62],

$$S_{\mathrm{E}} \propto \frac{c}{6}\log(\xi), \qquad \xi = -\frac{1}{\ln(e_2)}. \tag{A6}$$

The above scaling relation helps us to calculate directly the central charges of the underlying model. So, we need to have some different values of correlation length and von-Neumann entropy to fit them according to Eq. (A6). Thus, to produce different values of correlation length and von-Neumann entropy, we change the size of iMPS matrices of the ground state and calculate for each matrix size, correlation length, and von-Neumann entropy.

It is also worth mentioning that there is another direct connection between the correlation length and the size of the iMPS matrices [55–57]:

$$\xi \propto \chi^{\frac{1}{\sqrt{\frac{12}{c}+1}}}. \tag{A7}$$

So both quantities, the correlation length and the size of the matrices, have an explicit scaling relation. Hence, one can be replaced with the other one throughout the paper.

The general scheme of the algorithm for our model is as follows. First, we formulate the model to get a 1D model with only NN interactions; we bundle every three particles on a triangle, as shown in the Fig. 1, into one unit cell with dimension 8. For instance, according to the definition in Eq. (3), the Kitaev Hamiltonian is written in the following form:

$$\mathcal{H}_{\mathcal{K}} = -J_v\sum_{\langle i,j\rangle}\Sigma(i)^{IxI}\Sigma(j)^{xxI} - J_p\sum_{\langle i,j\rangle}\Sigma(i)^{zzz}\Sigma(j)^{zII}. \tag{A8}$$

Similar expressions would be used for the Ising terms. The CPU time of the iDMRG algorithm is proportional to the square of the spin dimensions d^2. It is obvious that the calculation time needed to accomplish a simple iDMRG on the mentioned lattice (with $d = 8$) is much larger than iDMRG performed on a lattice with spin dimension 2. This is the main reason that we were unable to examine larger matrices for this model. For example, the necessary time for convergence was about a couple of weeks for a single run of matrix size $\chi = 128$, and close to critical region. The convergence criterion was a fixed point relation between the Λ generated at the current step with the Λ of the last step.

We have also examined the iDMRG for the one-dimensional NNN TFI model and compared the results with the corresponding one of the original ladder. The entanglement spectrum and hence the entropy was the same within the relative error of 10^{-5}.

APPENDIX B: SYMMETRY

A symmetry is defined as an operation, which leaves the model Hamiltonian invariant. These symmetries can form either an ordinary group or a projective one. However, if the ground state of the Hamiltonian does not respect the Hamiltonian symmetries, one concludes the phase is a symmetry-broken one. At the same time, the remaining symmetry groups can protect a phase due to their inequivalent projective representations, also known as symmetry fractionalization. These two properties can be used to assign a unique label to every possible phase of a system and to detect possible phase transition within this classification [28].

The ground state of the Kitaev ladder Hamiltonian ($\mathcal{H}_{\mathcal{K}}$) is doubly degenerate and both ground states are invariant under the operations of $\mathcal{X}$ and $\mathcal{Z}$ [defined in Eq. (4)]. The mutual symmetry operation $\mathcal{X}\times\mathcal{Z}$ defines a $\mathbb{Z}_2\times\mathbb{Z}_2$ symmetry, which protects the Kitaev ladder ground states. In other words, providing the symmetry is preserved, the Kitaev SPT phase cannot be adiabatically mapped to a fully product state.

To gain more insight on how the $\mathbb{Z}_2\times\mathbb{Z}_2$ symmetry group can serve to protect the degeneracy of the entanglement spectrum, and how we can express them numerically we need to explore the properties of the symmetry group in terms of iMPS representation. To preserve the $\mathbb{Z}_2\times\mathbb{Z}_2$ symmetry for an iMPS state, the following relation should be satisfied [63],

$$\sum_{s'} u_{ss'}(g)\Gamma^{s'}_{\alpha\alpha'} = U^\dagger(g)_{\alpha\beta}\Gamma^s_{\beta\beta'}U(g)_{\beta'\alpha'}, \tag{B1}$$

where $u(g)\in G, G = \{\Sigma^{Izz}, \Sigma^{xxx}, -\Sigma^{xyy}, \Sigma^{III}\}$ and g represents the index of group elements. To obtain U_g for all elements of the group G, we construct the following transfer matrix ($\widehat{T}^g$) for each element of group G,

$$\widehat{T}^g_{\alpha\alpha',\beta\beta'} = \sum_{s,s'}\left(\Gamma^s_{\alpha\beta}\Lambda_\beta\right)u(g)^{s,s'}\left(\Gamma^{s'}_{\alpha'\beta'}\Lambda_{\beta'}\right)^*. \tag{B2}$$

The symmetry represented by $u(g)$ on all sites is respected, if the largest eigenvalue of $\widehat{T}^g$ becomes equal to 1. Using Eq. (B1), one can show the corresponding eigenvector is simply $U_g^\dagger$ [31].

Generally, $U_g, U_{g'}$ may not always form a regular group but a projective one. To see this behavior we need to apply

the symmetries in different order and make use of the facts that $u(g)u(g') = u(g')u(g)$ and $u^2(g) = \mathbb{1}$. Using $u(g)u(g') = u(g')u(g)$, we conclude

$$\begin{aligned} u(g)u(g')\Gamma &= U_g U_{g'} \Gamma U_{g'}^\dagger U_g^\dagger, \\ u(g')u(g)\Gamma &= U_{g'} U_g \Gamma U_g^\dagger U_{g'}^\dagger, \\ \Rightarrow U_g U_{g'} &= e^{i\Omega_{gg'}} U_{g'} U_g, \end{aligned} \tag{B3}$$

where the phase $e^{i\Omega_{gg'}}$ is called "phase factor" (for simplicity we drop indices corresponding to summations). The property of $u^2(g) = \mathbb{1}$ results in $U^2(g) = e^{i\theta_g}\mathbb{1}$. Using Eq. (B3) and $U^2(g) = e^{i\theta_g}\mathbb{1}$, one can easily show that $e^{i\Omega_{gg'}}$ can only be ± 1. The signs introduce two different kind of orders, i.e., SPT and trivial orders. Throughout the SPT (trivial) phase, $e^{i\Omega_{gg'}} = -1(+1)$ and only upon quantum phase transition, the sign can change. The two signs also represent two inequivalent projective representations of $\mathbb{Z}_2 \times \mathbb{Z}_2$ symmetry.

One can exploit this property and define an order parameter $\mathcal{O}$ (called phase factor order parameter), which can serve to detect, by measuring the sign, which projective representation holds for a possible phase,

$$\mathcal{O} = \frac{1}{\chi}\mathrm{Tr}(U_g U_{g'} U_g^\dagger U_{g'}^\dagger). \tag{B4}$$

When the iMPS doesn't possess one of the symmetries in the group, the phase factor order parameter $\mathcal{O}$ is simply 0, demonstrating the symmetry-broken phase.

The proposed $\mathbb{Z}_2 \times \mathbb{Z}_2$ symmetry group is not just the symmetry for the Kitaev Hamiltonian, but it commutes with the Ising interactions as well. As a result the phase factor order parameter $\mathcal{O}$, can be a good quantity to observe the phase transition which kills the symmetry-protected phase. When the system is close to the Kitaev phase the phase factor order parameter has a negative sign, which shows the system is in a symmetry-protected state, but for the ferromagnetic phase, while Σ^{Izz} is still respected, Σ^{xxx} is no longer preserved and the phase operator order parameter suddenly drops to zero, as shown in Fig. 10.

[1] D. C. Tsui, H. L. Stormer, and A. C. Gossard, Two-dimensional magnetotransport in the extreme quantum limit, Phys. Rev. Lett. **48**, 1559 (1982).

[2] T. Hansson, V. Oganesyan, and S. Sondhi, Superconductors are topologically ordered, Annals of Physics **313**, 497 (2004).

[3] X. Chen, Z.-C. Gu, and X.-G. Wen, Local unitary transformation, long-range quantum entanglement, wave function renormalization, and topological order, Phys. Rev. B **82**, 155138 (2010).

[4] C. Nayak, S. H. Simon, A. Stern, M. Freedman, and S. Das Sarma, Non-abelian anyons and topological quantum computation, Rev. Mod. Phys. **80**, 1083 (2008).

[5] A. Kitaev, Fault-tolerant quantum computation by anyons, Annals of Physics **303**, 2 (2003).

[6] X. G. Wen and Q. Niu, Ground-state degeneracy of the fractional quantum hall states in the presence of a random potential and on high-genus riemann surfaces, Phys. Rev. B **41**, 9377 (1990).

[7] X.-G. Wen, *Quantum field theory of many-body systems: From the origin of sound to an origin of light and electrons* (Oxford University Press, Oxford, 2007).

[8] H. Bombin and M. A. Martin-Delgado, Topological quantum distillation, Phys. Rev. Lett. **97**, 180501 (2006).

[9] H. Bombin and M. A. Martin-Delgado, Exact topological quantum order in $d = 3$ and beyond: Branyons and brane-net condensates, Phys. Rev. B **75**, 075103 (2007).

[10] H. Bombin and M. A. Martin-Delgado, Optimal resources for topological two-dimensional stabilizer codes: Comparative study, Phys. Rev. A **76**, 012305 (2007).

[11] M. Kargarian, Entanglement properties of topological color codes, Phys. Rev. A **78**, 062312 (2008).

[12] A. Kitaev and J. Preskill, Topological entanglement entropy, Phys. Rev. Lett. **96**, 110404 (2006).

[13] M. Levin and X.-G. Wen, Detecting topological order in a ground state wave function, Phys. Rev. Lett. **96**, 110405 (2006).

[14] K. P. Schmidt, S. Dusuel, and J. Vidal, Emergent fermions and anyons in the kitaev model, Phys. Rev. Lett. **100**, 057208 (2008).

[15] S. Dusuel, K. P. Schmidt, and J. Vidal, Creation and manipulation of anyons in the kitaev model, Phys. Rev. Lett. **100**, 177204 (2008).

[16] H. Bombin, M. Kargarian, and M. A. Martin-Delgado, Interacting anyonic fermions in a two-body color code model, Phys. Rev. B **80**, 075111 (2009).

[17] M. Kargarian, Finite-temperature topological order in two-dimensional topological color codes, Phys. Rev. A **80**, 012321 (2009).

[18] M. Kamfor, S. Dusuel, J. Vidal, and K. P. Schmidt, Spectroscopy of a topological phase, Phys. Rev. B **89**, 045411 (2014).

[19] K. P. Schmidt, Persisting topological order via geometric frustration, Phys. Rev. B **88**, 035118 (2013).

[20] S. Dusuel, K. P. Schmidt, J. Vidal, and R. L. Zaffino, Perturbative study of the kitaev model with spontaneous time-reversal symmetry breaking, Phys. Rev. B **78**, 125102 (2008).

[21] V. Karimipour, L. Memarzadeh, and P. Zarkeshian, Kitaev-ising model and the transition between topological and ferromagnetic order, Phys. Rev. A **87**, 032322 (2013).

[22] J. Vidal, S. Dusuel, and K. P. Schmidt, Low-energy effective theory of the toric code model in a parallel magnetic field, Phys. Rev. B **79**, 033109 (2009).

[23] J. Vidal, R. Thomale, K. P. Schmidt, and S. Dusuel, Self-duality and bound states of the toric code model in a transverse field, Phys. Rev. B **80**, 081104 (2009).

[24] S. S. Jahromi, M. Kargarian, S. F. Masoudi, and K. P. Schmidt, Robustness of a topological phase: Topological color code in a parallel magnetic field, Phys. Rev. B **87**, 094413 (2013).

[25] S. S. Jahromi, S. F. Masoudi, M. Kargarian, and K. P. Schmidt, Quantum phase transitions out of a $\mathbb{z}_2 \times \mathbb{z}_2$ topological phase, Phys. Rev. B **88**, 214411 (2013).

[26] F. Pollmann, A. M. Turner, E. Berg, and M. Oshikawa, Entanglement spectrum of a topological phase in one dimension, Phys. Rev. B **81**, 064439 (2010).

[27] X. Chen, Z.-C. Gu, and X.-G. Wen, Classification of gapped symmetric phases in one-dimensional spin systems, Phys. Rev. B **83**, 035107 (2011).

[28] X. Chen, Z.-C. Gu, and X.-G. Wen, Complete classification of one-dimensional gapped quantum phases in interacting spin systems, Phys. Rev. B **84**, 235128 (2011).

[29] R. Haghshenas, A. Langari, and A. T. Rezakhani, Symmetry fractionalization: Symmetry-protected topological phases of the bond-alternating spin-1/2 heisenberg chain, J. Phys.: Condens. Matter **26**, 456001 (2014).

[30] Projective representation of a specific symmetry group, e.g., G is accompanied by a phase factor. For instance, if elements g,g' and $g'' \in G$ have the relation $gg' = g''$, the corresponding projective representation becomes $U_g U_{g'} = e^{i\theta} U_{g''}$.

[31] F. Pollmann and A. M. Turner, Detection of symmetry-protected topological phases in one dimension, Phys. Rev. B **86**, 125441 (2012).

[32] C.-Y. Huang, X. Chen, and F. Pollmann, Detection of symmetry-enriched topological phases, Phys. Rev. B **90**, 045142 (2014).

[33] M. P. Zaletel, Detecting two-dimensional symmetry-protected topological order in a ground-state wave function, Phys. Rev. B **90**, 235113 (2014).

[34] L. Balents, Spin liquids in frustrated magnets, Nature (London) **464**, 199 (2010).

[35] C. Arizmendi, A. Rizzo, L. Epele, and C. García Canal, Phase diagram of the annni model in the hamiltonian limit, Zeitschrift für Physik B Condensed Matter **83**, 273 (1991).

[36] P. Sen, S. Chakraborty, S. Dasgupta, and B. Chakrabarti, Numerical estimate of the phase diagram of finite annni chains in transverse field, Zeitschrift für Physik B Condensed Matter **88**, 333 (1992).

[37] H. Rieger and G. Uimin, The one-dimensional annni model in a transverse field: Analytic and numerical study of effective hamiltonians, Zeitschrift für Physik B Condensed Matter **101**, 597 (1996).

[38] R. Derian, A. Gendiar, and T. Nishino, Modulation of local magnetization in two-dimensional axial-next-nearest-neighbor ising model, Journal of the Physical Society of Japan **75**, 114001 (2006).

[39] M. Beccaria, M. Campostrini, and A. Feo, Density-matrix renormalization-group study of the disorder line in the quantum axial next-nearest-neighbor ising model, Phys. Rev. B **73**, 052402 (2006).

[40] M. Beccaria, M. Campostrini, and A. Feo, Evidence for a floating phase of the transverse annni model at high frustration, Phys. Rev. B **76**, 094410 (2007).

[41] A. K. Chandra and S. Dasgupta, Floating phase in the one-dimensional transverse axial next-nearest-neighbor ising model, Phys. Rev. E **75**, 021105 (2007).

[42] A. K. Chandra and S. Dasgupta, Floating phase in a $2d$ annni model, Journal of Physics A: Mathematical and Theoretical **40**, 6251 (2007).

[43] A. Nagy, Exploring phase transitions by finite-entanglement scaling of MPS in the 1D ANNNI model, New Journal of Physics **13**, 023015 (2011).

[44] A. Kitaev, Anyons in an exactly solved model and beyond, Annals of Physics **321**, 2 (2006), January Special Issue.

[45] X.-Y. Feng, G.-M. Zhang, and T. Xiang, Topological characterization of quantum phase transitions in a spin-1/2 model, Phys. Rev. Lett. **98**, 087204 (2007).

[46] G. Kells, J. K. Slingerland, and J. Vala, Description of kitaev's honeycomb model with toric-code stabilizers, Phys. Rev. B **80**, 125415 (2009).

[47] W. DeGottardi, D. Sen, and S. Vishveshwara, Topological phases, majorana modes and quench dynamics in a spin ladder system, New Journal of Physics **13**, 065028 (2011).

[48] U. Schollwöck, The density-matrix renormalization group in the age of matrix product states, Annals of Physics **326**, 96 (2011).

[49] G. Vidal, Classical simulation of infinite-size quantum lattice systems in one spatial dimension, Phys. Rev. Lett. **98**, 070201 (2007).

[50] I. P. McCulloch, Infinite size density matrix renormalization group, revisited, arXiv:0804.2509.

[51] V. Karimipour, Complete characterization of the spectrum of the kitaev model on spin ladders, Phys. Rev. B **79**, 214435 (2009).

[52] J. Haegeman, D. Perez-Garcia, I. Cirac, and N. Schuch, Order parameter for symmetry-protected phases in one dimension, Phys. Rev. Lett. **109**, 050402 (2012).

[53] E. Lieb, T. Schultz, and D. Mattis, Two soluble models of an antiferromagnetic chain, Annals of Physics **16**, 407 (1961).

[54] M. Karbach, G. Müller, and K. Wiele, Interaction and thermodynamics of spinons in the XX chain, Journal of Physics A: Mathematical and Theoretical **41**, 205002 (2008).

[55] F. Pollmann, S. Mukerjee, A. M. Turner, and J. E. Moore, Theory of finite-entanglement scaling at one-dimensional quantum critical points, Phys. Rev. Lett. **102**, 255701 (2009).

[56] J. A. Kjäll, M. P. Zaletel, R. S. K. Mong, J. H. Bardarson, and F. Pollmann, Phase diagram of the anisotropic spin-2 XXZ model: Infinite-system density matrix renormalization group study, Phys. Rev. B **87**, 235106 (2013).

[57] P. Calabrese and J. Cardy, Entanglement entropy and quantum field theory, J. Stat. Mech.: Theor. Exp. (2004) P06002.

[58] F. Verstraete and J. I. Cirac, Matrix product states represent ground states faithfully, Phys. Rev. B **73**, 094423 (2006).

[59] M. B. Hastings, Locality in quantum and markov dynamics on lattices and networks, Phys. Rev. Lett. **93**, 140402 (2004).

[60] R. Orús and G. Vidal, Infinite time-evolving block decimation algorithm beyond unitary evolution, Phys. Rev. B **78**, 155117 (2008).

[61] H.-Q. Zhou, R. Orús, and G. Vidal, Ground state fidelity from tensor network representations, Phys. Rev. Lett. **100**, 080601 (2008).

[62] C. Sanderson, Armadillo: An Open Source C++ Linear Algebra Library for Fast Prototyping and Computationally Intensive Experiments. Technical Report, NICTA, 2010.

[63] M. Sanz, M. M. Wolf, D. Perez-Garcia, and J. I. Cirac, Matrix product states: Symmetries and two-body hamiltonians, Phys. Rev. A **79**, 042308 (2009).